Modeling the atomic structure of an amorphous $NiZr_3$ alloy by anomalous wide angle x-ray scattering and reverse Monte Carlo simulation

2008 J. Phys.: Condens. Matter 20 115103

(http://iopscience.iop.org/0953-8984/20/11/115103)

J. Phys.: Condens. Matter **20** (2008) 115103 (8pp) doi:10.1088/0953-8984/20/11/115103

Modeling the atomic structure of an amorphous $NiZr_3$ alloy by anomalous wide angle x-ray scattering and reverse Monte Carlo simulation

J C de Lima[1,3], D Raoux[1,4], Y Charriere[1] and M Maurer[1,2]

[1] LURE Bâtiment 209D, Faculté des Sciences, Orsay 91405, France
[2] Institut de Physique Nucleaire de Strasbourg, France

Received 15 June 2007, in final form 25 January 2008
Published 20 February 2008
Online at stacks.iop.org/JPhysCM/20/115103

Abstract

The amorphous atomic structure of a melt-spun $NiZr_3$ alloy was investigated using the anomalous wide angle x-ray scattering (AWAXS) and reverse Monte Carlo (RMC) simulation techniques. The AWAXS data were collected at four incident photon energies, including ones close to the Ni and Zr K-edges, and four total structure factors $S(K)$ were derived. Differential structure factors DAS(K) around the Ni and Zr atoms were calculated through the difference between the scattered intensities on a per-atom scale obtained at incident photon energy pairs (8330, 9455 eV) and (15622, 17993 eV). The contribution of the partial $S_{\mathrm{Ni-Ni}}(K)$ for the Ni-DAS(K) factor is six times bigger than the one for the $S(K)$ factors. Then, the use of the Ni-DAS(K) factor with four $S(K)$ factors as input data for the RMC simulations has permitted us to obtain more stable partial $S_{\mathrm{Ni-Ni}}(K)$, $S_{\mathrm{Ni-Zr}}(K)$ and $S_{\mathrm{Zr-Zr}}(K)$ factors. The partial $S_{ij}(K)$ factors are very close to those reported earlier for the amorphous $NiZr_2$ alloy. The structural data (coordination numbers and interatomic distances) for the first neighbors for both amorphous $NiZr_2$ and $NiZr_3$ alloys are also very similar.

1. Introduction

The physical properties of amorphous materials are strongly dependent on the configuration of the first neighbors. Due to absence of long-range order in these materials, the determination of their local atomic structures is a difficult task and it has been overcome through the combination of different diffraction and spectroscopic techniques and also simulation and modeling.

From a fundamental point of view, the Ni–Zr system has been attracting attention because amorphous phases, with different chemical compositions can be produced using different techniques such as melting spinning, mechanical alloying, etc. Thus, it offers an opportunity to study the evolution of the local atomic structure of Ni_xZr_{1-x} alloys with increasing Ni content and also to compare the local atomic structures present in a particular amorphous alloy prepared by different techniques.

The atomic structure of amorphous alloys containing N chemical elements is described by $N(N+1)/2$ pair correlation functions $G_{ij}(r)$ that are related to the total structure factor $S(K)$ through a Fourier transformation. Thus, to obtain the $N(N+1)/2$ $G_{ij}(r)$ functions, we need $N\{N+1)/2$ independent $S(K)$ factors. For a binary alloy, the three independent $S(K)$ can be obtained through the following techniques: (1) isomorphous substitution [1], (2) isotope substitution [2], and (3) anomalous wide angle x-ray scattering (AWAXS) [3, 4]. The use of AWAXS consists of turning the energy of the incident x-ray beam close to the K-edge of a specific atom of the alloy and promoting a resonant interaction with the electrons of that atom. For example, for an amorphous Ni_xZr_{1-x} alloy, the three independent $S(K)$ factors can be measured selecting energies close and away from the K-edges of Ni and Zr atoms. However, the matrix formed by the weights of the three $S(K)$ factors is ill-conditioned, a fact that compromises the determination

[3] Permanent address: Physics Department, Universidade Federal de Santa Catarina, 88040-900 Florianopolis, Santa Catarina, Brazil.
[4] Permanent address: Synchrotron SOLEIL-L'Orme des Merisiers Saint-Auban–BP 48 91192 Gif-sur-Yvette cedex, France.

of the partial $S_{\mathrm{Ni-Ni}}(K)$, $S_{\mathrm{Ni-Zr}}(K)$ and $S_{Zr-Zr}(K)$ structure factors.

Trying to overcome this difficulty, Fuoss and co-workers [3, 4] implemented the differential anomalous scattering (DAS) approach proposed by Schevchik [5, 6]. A differential anomalous scattering factor DAS(K) can be obtained from the AWAXS measurements performed at two energies just below the K-edge of a selected atom making the difference between the normalized scattered intensities on a per-atom scale (see equation (5) below). This factor describes the chemical environment around this atom because all the correlations not involving this atom cancel out since only its atomic scattering factor changes appreciably.

Almost two decades ago, de Lima and co-workers used the DAS approach to study a melt-spun amorphous $NiZr_3$ alloy. The results were reported in [7]. Later, in another study, de Lima *et al* [8] following a suggestion by Munro [9], used a combination of AWAXS $S(K)$ and DAS(K) factors measured for an amorphous $Ni_{64}Zr_{36}$ alloy together with the matrix inversion method to obtain more stable $S_{\mathrm{Ni-Ni}}(K)$, $S_{\mathrm{Ni-Zr}}(K)$ and $S_{\mathrm{Zr-Zr}}(K)$ structure factors. The $S_{ij}(K)$ factors agreed very well with those obtained previously for the same sample using the isotope substitution and neutron diffraction techniques [10]. The combination of $S(K)$ and DAS(K) factors substantially reduced the conditioning number of the matrix formed by the weights [11] of the factors. Later, the same procedure was applied to the amorphous $NiZr_3$ alloy, in which the maximum contribution of the $S_{\mathrm{Ni-Ni}}(K)$ factor was smaller than 5% for the $S(K)$ factors. Its contribution reached 18% for the Ni-DAS(K) factor. The $S_{\mathrm{Zr-Zr}}(K)$ factor obtained showed a high stability, while the $S_{\mathrm{Ni-Ni}}(K)$ and $S_{\mathrm{Ni-Zr}}(K)$ presented an instability in the low-K range.

The reverse Monte Carlo (RMC) simulation method has been successfully used for structural modeling of amorphous structures. This method uses $S(K)$ factors derived from neutron and/or x-ray measurements. Recently, de Lima *et al* [12] modeled the amorphous structure of an amorphous $NiZr_2$ alloy using the RMC method and AWAXS $S(K)$ factors as input data. In that alloy, the maximum contribution of the $S_{\mathrm{Ni-Ni}}(K)$ factor was of 10% for the $S(K)$ factors. The $S_{\mathrm{Ni-Ni}}(K)$, $S_{\mathrm{Ni-Zr}}(K)$ and $S_{\mathrm{Zr-Zr}}(K)$ structure factors agreed very well with those reported in the literature [2], showing that the RMC method is appropriate to investigate dilute binary amorphous alloys.

The excellent results obtained for the amorphous $NiZr_2$ alloy motivated us to apply the RMC simulations to the amorphous $NiZr_3$ alloy studied previously using the DAS approach [7]. Another important point is the contribution of the $S_{\mathrm{Ni-Ni}}(K)$ factor for the Ni-DAS(K) factor (≈18%), suggesting that more stable $S_{\mathrm{Ni-Ni}}(K)$, $S_{\mathrm{Ni-Zr}}(K)$ and $S_{\mathrm{Zr-Zr}}(K)$ factors can be obtained if the $S(K)$ and Ni-DAS(K) factors are used together as input data. The literature does not report studies involving the use of the DAS(K) factor as input data for the RMC simulations. Thus, the aim of this paper is to report the partial $S_{ij}(K)$ factors obtained considering the $S(K)$ and Ni-DAS(K) factors as input data.

2. Theoretical background

2.1. Total and partial structure factors

According to Faber and Ziman [13], $S(K)$ is obtained for a binary alloy from the normalized scattered intensity on a per-atom scale $I_{\mathrm{a}}(K)$ as follows:

$$S(K) = \frac{I_{\mathrm{a}}(K) - [\langle f^2(K)\rangle - \langle f(K)\rangle^2]}{\langle f(K)\rangle^2} \tag{1}$$

$$= \sum_{i,j=1}^{2} W_{ij}(K) S_{ij}(K), \tag{2}$$

where K is the transferred momentum and $W_{ij}(K)$ are the weights of the $S_{ij}(K)$ factors, which are given by

$$W_{ij}(K) = \frac{c_i c_j f_i(K) f_j(K)}{\langle f(K)\rangle^2}, \tag{3}$$

$$\langle f^2(K)\rangle = \sum_i c_i f_i^2(K),$$

and

$$\langle f(K)\rangle^2 = \left[\sum_i c_i f_i(K)\right]^2.$$

Here, $K = \frac{4\pi \sin\theta}{\lambda}$, c_i is the concentration, $f_i(K, E) = f_0(K) + f'(E) + if''(E)$ is the atomic scattering factor, and $f'(E)$ and $f''(E)$ are the anomalous dispersion terms.

The $G_{ij}(r)$ functions are related to the $S_{ij}(K)$ through a Fourier transformation

$$G_{ij}(r) = 1 + (1/2\pi^2\rho_0 r)\int_0^\infty K[S_{ij}(K) - 1]\sin(Kr)\,\mathrm{d}K. \tag{4}$$

From the first maxima of the $G_{ij}(r)$ functions the interatomic distances for the first neighbors are obtained.

2.2. Differential structure factor

Using the Faber–Ziman formalism [13], the DAS (K, E_m, E_n) factor about a selected atom of the alloy is obtained as follows

$$\mathrm{DAS}(K, E_m, E_n) = \frac{[I_{\mathrm{a}}(K, E_m) - I_{\mathrm{a}}(K, E_n)] - [LS(K, E_m) - LS(K, E_n)]}{\langle f(K, E_m)\rangle^2 - \langle f(K, E_n)\rangle^2} \tag{5}$$

$$= \sum_j U_{ij}(K, E_m, E_n) S_{ij}(K), \tag{6}$$

where $LS(K, E) = \langle f^2(K, E)\rangle - \langle f(K, E)\rangle^2$ is the Laue scattering term and

$$U_{ij}(K, E_m, E_n) = \frac{c_i c_j [f_i(K, E_m) f_j(K, E_m) - f_i(K, E_n) f_j(K, E_n)]}{\langle f(K, E_m)\rangle^2 - \langle f(K, E_n)\rangle^2}. \tag{7}$$

For $i \neq j$ the weight $U_{ij}(K, E_m, E_n)$ must be multiplied by 2. The letters m and n mean the incident photon energies just below the K-edge of the selected atom. For amorphous Ni_xZr_{1-x} alloys, the Ni-DAS(K) and Zr-DAS(K) factors contain structural information regarding the $S_{\mathrm{Ni-Ni}}(K) + S_{\mathrm{Ni-Zr}}(K)$ and $S_{\mathrm{Zr-Zr}}(K) + S_{\mathrm{Zr-Ni}}(K)$ factors, respectively.

2.3. Reverse Monte Carlo method

The paper by Tucker *et al* [14] gives an excellent review of the RMC method and its application to crystalline and amorphous materials.

The RMC method is based on statistical mechanics, and its basic idea and the algorithm are described elsewhere (see articles cited in [12]). Its application for modeling the structure of noncrystalline materials uses as a starting point one or more experimental $S(K)$ factors, and has the purpose of generating static atomic configurations by a procedure explicitly designed to give the best agreement with experimental data. It bypasses the need for representations of the interatomic forces or atomic potentials. The best match between the simulated and experimental $S(K)$ factors indicates that the static atomic configuration generated may be close to reality and may also allow an understanding of the atomic structure as well as the search for insights behind the raw data. In order to obtain the most consistent atomic configurations, more than one $S(K)$ factor should be used.

The RMC method takes into account the effects of experimental resolution [14]. Thus, it is important to determine the experimental $S(K)$ factors in a K-range as large as possible (typically 50 Å^{-1}) in order to achieve the best possible resolution in the $G(r)$ function. According to the sampling theorem, the resolution Δr is given as $\pi/K_{\max}$, where $K_{\max}$ is the maximum value of K achieved in the measurement of $S(K)$.

The forward Fourier transforms of the $K[S(K) - 1]$ to obtain the $G(r)$ function is straightforward, but it is subject to a problem that arises from the fact that the data for $S(K)$ extend only to some maximum value of K. The effect of the finite range of K on the Fourier transform is to introduce spurious ripple peaks in the computed $G(r)$ function. This problem can be avoided by multiplying $K[S(K) - 1]$ by the Lorch function $M(K) = \frac{\sin(\pi K/K_{\max})}{\pi K/K_{\max}}$ [15], which decreases smoothly to zero at $K_{\max}$. However, the Fourier transform of the modified form of $K[S(K) - 1]$ will then be convoluted with the Fourier transform of $M(K)$, artificially broadening the peaks in the $G(r)$ function. In order to overcome this problem the RMC method can be used to obtain a $G(r)$ function whose Fourier transform best matches the experimental $K[S(K) - 1]$ data. It is important to note that although the spurious ripple peaks into the computed $G(r)$ function are overcome the effects of experimental resolution remain.

The starting point when using the RMC method to study noncrystalline materials is to generate an initial configuration of atoms (a random distribution of atoms) without unreasonably short interatomic distances. An RMC simulation will evolve to maximize the amount of disorder (entropy) in the configurations generated. Thus, it will give the most disordered atomic configurations that are consistent with the experimental data. There may be a range of configurations that match the data, with different degrees of disorder. Only by maximizing the range of experimental data can this problem be minimized. In order to obtain the most disordered final atomic configuration that is consistent with the experimental data, two preliminary procedures are commonly used: (i) in the initial atomic configuration, at the beginning, minimum approach (cutoff) distances Δ_{ij} between the atomic centers are fixed to act as constraints on the short-range structure, and (ii) entropy maximization of the atomic configuration. This step ensures that the model will not be trapped in a local minimum and will, instead, converge on the global minimum.

The individual pair distribution $G_{ij}(r)$ functions are defined as

$$G_{ij}(r) = \frac{N_{ij}(r)}{4\pi\rho_0 r^2 \Delta r},$$

where $N_{ij}(r)$ is the number of atoms of type j lying within the range of distances between r and $r + \mathrm{d}r$ from any atom of type i, and $\rho_i = c_i\rho_0$.

During the RMC simulation process the following function is minimized:

$$\psi^2 = \frac{1}{\delta}\sum_{i=1}^{m}[S^{\mathrm{RMC}}(K_i) - S(K_i)]^2.$$

The sum is over m experimental points and δ is related to the experimental error in $S(K)$. In order to minimize the Ψ function, atoms are selected at random and moved small random distances. If the move reduces Ψ, it is accepted. If the move increases Ψ, it is accepted with the probability

$$P = \exp(-\Delta\psi^2/2).$$

As the process is iterated Ψ^2 decreases until it reaches a global equilibrium value. Thus, in principle, the final atomic configuration corresponding to the equilibrium is the most disordered and consistent with the experimental data. Using the $G_{ij}(r)$ and $S_{ij}(K)$ functions corresponding to the final atomic configuration, the coordination numbers, interatomic distances and bond-angle distributions can be calculated.

3. Experimental procedure

Melt-spun amorphous $NiZr_3$ ribbons ≈30 μm thick and 1 mm wide were prepared. The measured density of the ribbons was $\rho = 7.40$ g cm^{-3} or 0.05364 atoms Å^{-3}. For the AWAXS measurements, several ribbons were carefully aligned and glued on a metallic holder with a central rectangular hole to make a sample.

The AWAXS measurements were performed at the LURE (Orsay, France), in 1985, using the DCI synchrotron radiation source. The experimental conditions were the same as used for the amorphous $NiZr_2$ alloy, which are detailed in [12]. The sample was not in a vacuum during the AWAXS measurements. In order to subtract the contribution of the air scattering in the low-K range for the AWAXS measurements, an air scattering pattern was measured and the procedure described in [16] was used. The data reduction procedure is described in [12] and will not be repeated here. The RMC package program (version 3) was downloaded from the site http://www.studsvik.uu.se.

4. Results and discussion

The $S(K)$ factors measured at incident photon energies of 15622 and 17993 eV reached a value of $K_{\max} = 15.45$ Å^{-1},

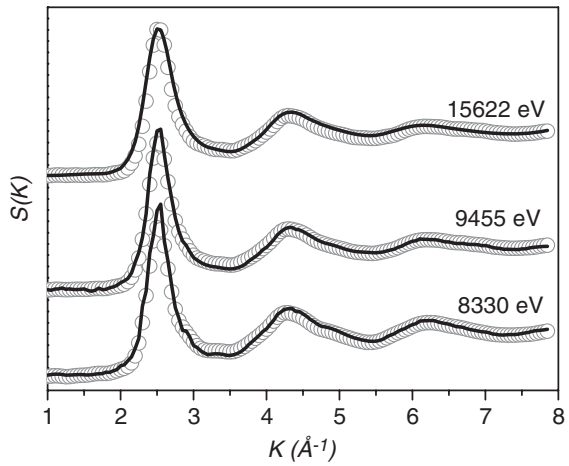

Figure 1. AWAXS total structure factors $S(K)$: experimental (thick solid lines) and simulated (open circle lines).

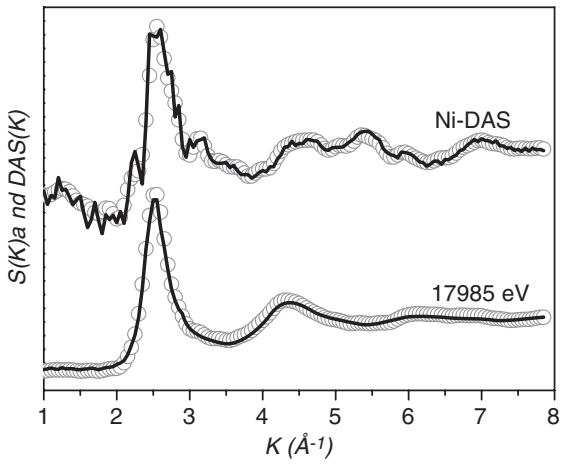

Figure 2. AWAXS total structure $S(K)$ and Ni-DAS(K) factors: experimental (thick solid lines) and simulated (open circle lines).

while the values for those measured at 8330 and 9455 eV were 7.80 and 9 Å^{-1}, respectively. Thus, the best resolution reached in the $G(r)$ function was $\Delta r \approx 0.21$ Å. However, in order to obtain the best consistent atomic configuration, the Ni-DAS (K) and $S(K)$ factors will be used as input data for the RMC simulations. For that, the factors must have the same K-range ($K_{\max} = 7.80$ Å^{-1}), reducing the resolution of the $G(r)$ function for $\Delta r \approx 0.40$ Å.

Figures 1 and 2 show the $S(K)$ and Ni-DAS(K) factors (thick solid lines) measured for the incident photon energies listed in table 1. This table also gives the values of the anomalous dispersion $f'(E)$ and $f''(E)$ for each energy used in the AWAXS measurements. The Ni-DAS(K) factor was calculated using the normalized scattered intensities on a per-atom scale obtained at the incident photon energy pair (9455, 8330 eV) and following equation (5). This factor is the same as reported in [16]. The $S(K)$ factors are a weighted sum of the $S_{\mathrm{Ni-Ni}}(K)$, $S_{\mathrm{Ni-Zr}}(K)$ and $S_{\mathrm{Zr-Zr}}(K)$ factors, while the Ni-DAS(K) factor is a weighted sum involving only the $S_{\mathrm{Ni-Ni}}(K)$, $S_{\mathrm{Ni-Zr}}(K)$ factors. The values of the weights $W_{ij}(K)$ and $U_{ij}(K, E_m, E_n)$ depend on the incident photon energy through the atomic scattering factor $f_i(K)$ of the Ni and Zr atoms. The smallest and greatest contributions of the $S_{\mathrm{Ni-Ni}}(K)$ factor for the $S(K)$ factors occur at energies of 8330 and 17993 eV, respectively, while the opposite occurs with $S_{\mathrm{Zr-Zr}}(K)$. Thus, the present changes in these $S(K)$ factors are associated with changes in the $f'(E)$ and $f''(E)$ values, mainly with the $f'(E)$ term. At $K = 1.0$ Å^{-1}, the maximum contributions of the $S_{\mathrm{Ni-Ni}}(K)$, $S_{\mathrm{Ni-Zr}}(K)$ and $S_{\mathrm{Zr-Zr}}(K)$ factors for the $S(K)$ factors are 5.4%, 35.6% and 74.7%, respectively, while the contribution of the $S_{\mathrm{Ni-Ni}}(K)$ factor for the Ni-DAS(K) factor is 18.3%. This last value suggests that more stable $S_{\mathrm{Ni-Ni}}(K)$ and $S_{\mathrm{Ni-Zr}}(K)$ factors can be obtained considering the $S(K)$ and Ni-DAS(K) factors as input data for the RMC simulations. In order to evaluate the influence of the Ni-DAS(K) factor in the simulated structure, we separated the input data in two sets, and they were considered separately. The first set is only formed by the four $S(K)$ factors, while the second one comprises the four $S(K)$ and Ni-DAS(K) factors.

Table 1. Incident photon energy and f', f'' values.

Energy (eV)	f'_{Ni}	f''_{Ni}	f'_{Zr}	f''_{Zr}
8 330	−7.866	1.206	−0.366	2.113
9 455	−1.416	3.158	−0.554	1.692
15 622	0.245	1.346	−1.822	0.679
17 993	0.269	1.056	−7.769	1.227

For the RMC simulations, the density value $\rho_0 = 0.05364$ atoms Å^{-3} (7.40 g cm^3) and 5000 atoms (1250 Ni and 3750 Zr) were used to generate an initial random configuration, without unreasonably short interatomic distances, into a cubic box of edge $L = 45$ Å. It is well known that the $G_{ij}(r)$ functions have the first neighbor shells well represented by one or more Gaussian functions. With the exception of the pre-peaks associated with the chemical intermediate range order, those located before the first shell have no physical meaning. These features should be pursued in any method used for modeling the atomic structure of amorphous materials. The literature reports that the amorphous Ni–Zr alloys show pre-peaks [8, 11, 12]. We have assumed cutoff distances Δ_{ij} in the RMC simulations to act as constraints on the short-range structure, and these were carefully investigated. In the absence of a direct Fourier transform, there are no criteria for choosing them; however, some physical considerations about the types of atoms as well as their contents in the alloy may be useful [17]. The atomic radii of Ni and Zr atoms are 1.25 Å and 1.60 Å, respectively; the Ni content in the amorphous $NiZr_3$ alloy is 25 at.% (diluted alloy). Thus, the value of $\Delta_{\mathrm{Ni-Ni}}$ may be greater than those of $\Delta_{\mathrm{Ni-Zr}}$ and $\Delta_{\mathrm{Zr-Zr}}$. Based on these considerations, several sets of cutoff distances Δ_{ij} were examined. Each Δ_{ij} set was introduced in the initial random configuration before it was submitted to a process to maximize the amount of disorder (entropy). This process is well described in the RMC manual. After this, the configuration and the $S(K)$ and Ni-DAS(K) factors were used for the RMC simulation [18].

For the second input data set, the best simulations were reached considering the $\Delta_{\mathrm{Ni-Ni}} = 2.30$ Å and $\Delta_{\mathrm{Ni-Zr}} =$

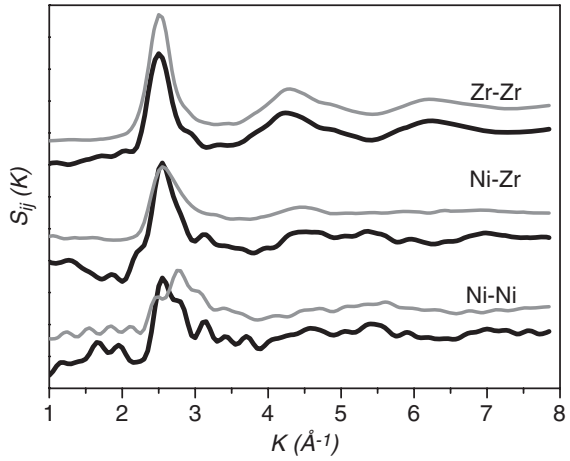

Figure 3. Partial structure factors $S_{ij}(K)$ obtained using the four $S(K)$ and the Ni-DAS(K) factors (thick black lines) and only the four $S(K)$ factors (thick gray lines).

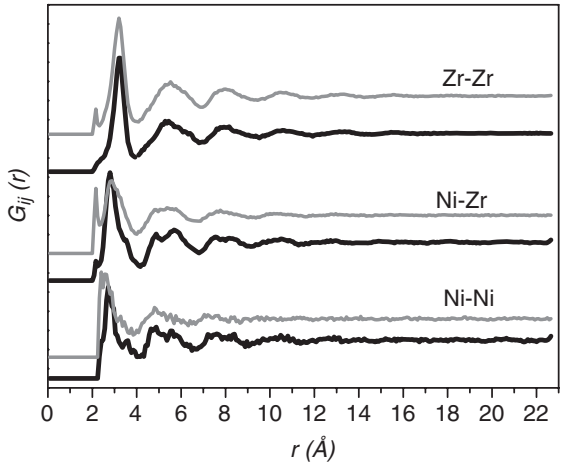

Figure 4. Partial distribution functions $G_{ij}(r)$ obtained using the four $S(K)$ and the Ni-DAS(K) factors (thick black lines) and just the four $S(K)$ factors (thick gray lines).

$\Delta_{\mathrm{Zr-Zr}} = 2.10$ Å values. In order to verify the influence of the Ni-DAS(K) factors for the results, these values were kept when the first input data set was considered. Also, to minimize possible errors related to the air subtraction procedure, the RMC simulations were only performed considering K ranging from 1 to 7.80 $\mathrm{Å}^{-1}$. The simulated $S(K)^{\mathrm{RMC}}$ and Ni-DAS$^{\mathrm{RMC}}(K)$ factors (open circle lines) are shown in figures 1 and 2, where one can see an excellent agreement with the experimental data.

Figure 3 shows the $S_{\mathrm{Ni-Ni}}(K)$, $S_{\mathrm{Ni-Zr}}(K)$ and $S_{\mathrm{Zr-Zr}}(K)$ factors obtained using the first (thick gray lines) and second (thick black lines) input data sets. A comparison of the $S_{ij}(K)$ factors obtained using these two input data sets shows that they have the same shapes and details. They differ only in the region located before the main peaks, where one can clearly see the presence of the pre-peaks related to the chemical intermediate order range. These pre-peaks are more intense in the $S_{ij}(K)$ factors obtained using the second input data set due to the higher contribution of the $S_{\mathrm{Ni-Ni}}(K)$ for the Ni-DAS(K) factor.

Figure 4 shows the $G_{\mathrm{Ni-Ni}}(r)$, $G_{\mathrm{Ni-Zr}}(r)$ and $G_{\mathrm{Zr-Zr}}(r)$ functions obtained using the first (thick gray lines) and second (thick black lines) input data sets. A comparison of the $G_{ij}(r)$ functions shows that the use of the second input data set ($S(K)$ and Ni-DAS(K) factors) gives functions that are clearly better defined, with the first neighbor shells totally defined and having no spurious peaks. From this figure one can also see that the first neighbor shells are well isolated. However, the shells related to the Ni–Ni and Ni–Zr neighbors are formed of sub-shells. That related to the Zr–Zr neighbors does not show sub-shells. It is interesting to note that the second and third neighbor shells of the $G_{\mathrm{Ni-Ni}}(r)$ and $G_{\mathrm{Ni-Zr}}(r)$ functions are split into two sub-shells, indicating the presence of chemical intermediate range order, while in the $G_{\mathrm{Zr-Zr}}(r)$ function this splitting is absent. The spurious peaks located at $r = 2.16$ Å are related to the assumed Δ_{ij} values. However, they do not influence the results. The interatomic distances for the first neighbors are those corresponding to the first maxima on the $G_{ij}(r)$ functions, and the coordination numbers were

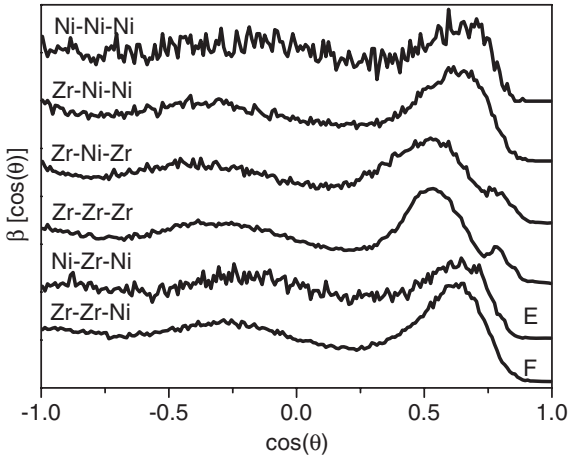

Figure 5. Distribution of the cosine of the bond-angles, $\beta[\cos(\theta)]$, for Ni–Ni–Ni, Zr–Ni–Zr, Zr–Ni–Ni, Zr–Zr–Zr, Ni–Zr–Ni and Zr–Zr–Ni, calculated using the final configuration obtained from the RMC simulations.

calculated from the final atomic configuration. For this, the upper limit values of 4.16, 4.16 and 3.92 Å for the Ni–Ni, Ni–Zr and Zr–Zr first shells were fixed. To establish error bars on the coordination numbers intermediate values were considered. The obtained values are listed in table 2.

It is known that the orientational correlations in disordered structures could be well represented by the distribution of the cosine of the bond-angles $\beta[\cos(\theta)]$. Bonds were defined by neighbors within the first coordination shell. In order to establish error bars on the bond-angle distributions, the same intermediate and upper limit values used to calculate the coordination numbers were applied. Figure 5 shows the Ni–Ni–Ni, Zr–Ni–Ni, Zr–Ni–Zr, Zr–Zr–Zr, Ni–Zr–Ni and Zr–Zr–Ni bond-angle distributions (the angle is centered at the middle atom) obtained from the final atomic configuration. From this figure one can see that the curves for the Ni–Ni–Ni and Ni–Zr–Ni cosine bond-angle distributions shows very poor statistics, suggesting that the coordination numbers corresponding to the

Table 2. Structural parameter values for the amorphous $NiZr_3$ alloy.

Structural parameters	N_{Ni-Ni}	r (Å)	N_{Ni-Zr}	r (Å)	N_{Zr-Zr}	r (Å)
This work	2.90 ± 0.74	2.72	9.42 ± 1.74	2.80	10.54 ± 0.10	3.20
a-$NiZr_3$ [7] (DAS)	$\leqslant 1.30$	$\leqslant 4.10$	3.00[a] 6.00	2.76 3.04	0.56[c] 2.50 7.60	2.76 3.04 3.40
a-$NiZr_3$ [11] (Matrix inversion)	—	—	9.95	2.83	10.80	3.22
a-$NiZr_2$ [12]	3.20	2.68	6.90[b] 2.30	2.73 3.62	10.10	3.25
a-$Ni_{24.1}Zr_{75.9}$ [20]	—	—	14.50	2.70	8.40	3.16
c-$NiZr_2$ [21]	2.00	2.63	8.00	2.79	1.00[d] 2.00 4.00 4.00	2.82 3.17 3.30 3.47

[a] There are 9 Ni–Zr pairs at $\langle r \rangle = 2.95$ Å.
[b] There are 9.2 Zr–Zr pairs at $\langle r \rangle = 2.95$ Å.
[c] There are 10.66 Zr–Zr pairs at $\langle r \rangle = 3.28$ Å.
[d] There are 11 Zr–Zr pairs at $\langle r \rangle = 3.29$ Å.

first neighbors Ni–Ni and Zr–Ni are relatively small. The Ni–Ni–Ni, Zr–Ni–Zr and Zr–Ni–Ni bond-angle distribution curves show peaks centered at about the following values: $\cos(\theta) = -0.271 \pm 0.039$ ($\theta = 103.4°$–$108.1°$) and $\cos(\theta) = 0.576 \pm 0.049$ ($\theta = 51.3°$–$58.2°$); $\cos(\theta) = -0.470 \pm 0.049$ ($\theta = 114.9°$–$121.3°$) and $\cos(\theta) = 0.448 \pm 0.047$ ($\theta = 60.3°$–$66.4°$); $\cos(\theta) = -0.437 \pm 0.046$ ($\theta = 113.0°$–$118.9°$) and $\cos(\theta) = 0.550 \pm 0.058$ ($\theta = 52.5°$–$60.5°$), respectively, while Zr–Zr–Zr, Ni–Zr–Ni and Zr–Zr–Ni display peaks centered about $\cos(\theta) = -0.353 \pm 0.016$ ($\theta = 109.7°$–$111.6°$) and $\cos(\theta) = 0.512 \pm 0.011$ ($\theta = 58.5°$–$59.9°$); $\cos(\theta) = -0.230 \pm 0.015$ ($\theta = 102.4°$–$104.2°$) and $\cos(\theta) = 0.589 \pm 0.021$ ($\theta = 52.4°$–$55.4°$); $\cos(\theta) = -0.318 \pm 0.014$ ($\theta = 107.7°$–$109.4°$) and $\cos(\theta) = 0.585 \pm 0.020$ ($\theta = 52.8°$–$55.6°$), respectively. The triangle and ideal tetrahedral angles are $\theta = 60°$ and $109.5°$, respectively. In another paper [12], we modeled the amorphous structure of the $NiZr_2$ alloy through the RMC simulations. The bond-angle distribution curves reported in that paper are similar to those displayed in figure 5. Thus, the same physical interpretation given in that paper can be directly transported for the amorphous $NiZr_3$ alloy, and it will be not repeated here.

According to table 2, the Ni and Zr atoms have on average 14.8 (3.6 Ni–Ni + 11.2 Ni–Zr) and 14.3 (3.7 Zr–Ni + 10.6 Zr–Zr) nearest neighbors, respectively. These numbers indicate that the Ni and Zr atoms have equivalent roles on a topological network formed by spheres of very similar sizes. This evidence is supported by the similarity between the Zr–Zr–Zr and Zr–Ni–Zr bond-angle distribution curves shown in figure 5.

The chemical short-range order (CSRO) in the amorphous alloy is obtained using the Warren parameter α_w given by [19]

$$\alpha_w = 1.0 - \frac{N_{Ni-Zr}}{c_{Zr}[c_{Ni}(N_{Zr-Zr} + N_{Zr-Ni}) + c_{Zr}(N_{Ni-Ni} + N_{Ni-Zr})]},$$

where N_{ij} are the coordination numbers listed in table 2. The α_w parameter is null for a random distribution. If there is a preference for forming unlike pairs in the alloy, it becomes negative. Otherwise, it is positive if homopolar pairs are preferred. Using the N_{ij} for the amorphous $NiZr_3$ alloy given in table 2, the CSRO parameter was calculated, and the value found was $\alpha_w = -0.018$, suggesting a preference for formation of a random distribution.

It is interesting to compare the structural parameters (coordination numbers and interatomic distances) obtained for the amorphous $NiZr_3$ alloy using the RMC method with those reported earlier for the same alloy, which were obtained through the DAS approach [7] and matrix inversion method [11]. The structural parameters for the first neighbors obtained in those works are listed in table 2. In those works it was not possible to find the coordination number for the Ni–Ni pairs, while in the present study this number is precisely determined. The number of Ni–Zr pairs obtained in this study is slightly larger than those reported previously, and the number of Zr–Zr pairs is similar.

Due to closeness in composition of the amorphous $NiZr_2$ and $NiZr_3$ alloys, it is also interesting to compare the $S_{ij}(K)$ factors as well as the structural parameters found for these alloys. Figure 6 shows the $S_{ij}(K)$ factors obtained for amorphous $NiZr_2$ (thick gray lines) together with those obtained in this study (thick black lines). The structural parameters reported in [12] for the amorphous $NiZr_2$ alloy are listed in table 2. From figure 6 one can see that the

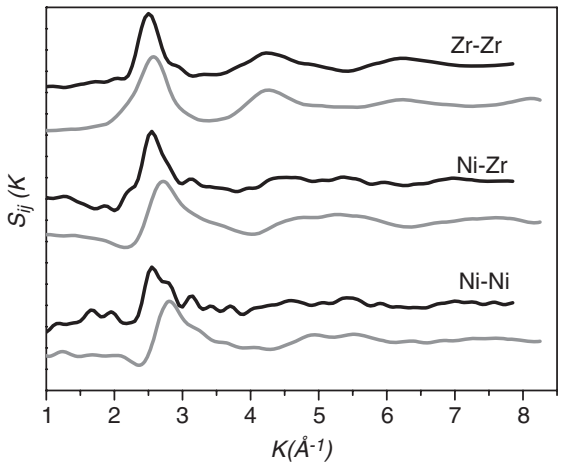

Figure 6. Partial structure factors $S_{ij}(K)$: for the amorphous $NiZr_3$ alloy (thick black lines) and for the amorphous $NiZr_2$ alloy (thick gray lines).

$S_{ij}(K)$ factors obtained for both amorphous $NiZr_2$ and $NiZr_3$ alloys are very similar. This similarity is also observed for the structural parameters.

Paul and Frahm [20] reported values for the structural parameters of an amorphous $Ni_{24.1}Zr_{75.9}$ alloy and they are listed in table 2. They did not report coordination numbers for the Ni–Ni first neighbors. We reported the same results in previous studies [7, 11]. The number of Ni–Zr pairs reported by them is substantially larger than those found in our works, while the opposite is found for the Zr–Zr pairs. The interatomic distances reported by them for the Ni–Zr and Zr–Zr pairs are similar to the average values found in our works.

Due to closeness in composition of crystalline $NiZr_2$ and amorphous $NiZr_3$ phases, some similarity between the short-range orders present in these phases may occur. Thus, it is interesting to compare these local atomic structures. For that, the structural data reported by Havinga *et al* [21] for the tetragonal $NiZr_2$ compound were used. These data and the CRYSTAL OFFICE 98 software[5] were used to calculate the coordination numbers, interatomic distances and bond-angles for the first neighbors. The calculated values for the coordination numbers and interatomic distances are listed in table 2. From this table one can see that the calculated interatomic distances for the crystalline $NiZr_2$ compound are similar to those found in this study. However, the numbers of Ni–Ni and Ni–Zr pairs present in the amorphous $NiZr_3$ phase are greater than those found in the crystalline $NiZr_2$ compound, while the number of Zr–Zr pairs is similar. The increase observed in the Ni–Ni and Ni–Zr coordination numbers may be associated with the amorphous phase density ($\rho = 7.40$ g cm^{-3}), which is 2.26% bigger than that for the crystalline compound ($\rho = 7.233$ g cm^{-3}).

[5] Atomic Softek, 70 Longwood Road North, Hamilton, Ontario, Canada L8S 3V4.

5. Conclusions

The amorphous $NiZr_3$ alloy was investigated using AWAXS, DAS, and RMC simulation techniques. Several conclusions are obtained from this study. The main ones are as follows.

The use of the Ni-DAS(K) factor together with the four AWAXS $S(K)$ factors as input data for the RMC simulations has permitted us to obtain more stable $S_{Ni-Ni}(K)$ and $S_{Ni-Zr}(K)$ factors. The obtained $S_{Ni-Ni}(K)$, $S_{Ni-Zr}(K)$ and $S_{Zr-Zr}(K)$ factors are very similar to those reported earlier for the amorphous $NiZr_2$ alloy. The structural data for the first neighbors for both amorphous $NiZr_2$ and $NiZr_3$ alloys are also very similar.

The results reported in this study show that the RMC method is appropriate for investigating dilute amorphous samples, in which the content of the minority chemical component is about of 25 at.%. However, due to the small contribution of the partial structure factor associated with the minority component for the $S(K)$ factors, whenever possible a DAS(K) factor around the K-edge of the minority component must be measured because its contribution to the DAS(K) factor is several times larger. The use of the DAS(K) and independent $S(K)$ factors as input data for the RMC simulation allows us to obtain more stable $S_{ij}(K)$ factors.

In another study, some resemblance was observed between the local atomic structures present in the tetragonal $NiZr_2$ and amorphous $NiZr_2$ phases. Now, we also observed some resemblance between the local atomic structures present in this crystal and the amorphous $NiZr_3$ phase.

Acknowledgments

One of the authors (J C de Lima) thanks Conselho Nacional de Desenvolvimento Cientifico e Tecnológico–CNPq (Brazil) for financial support. We thank Dr R S de Biasi for a careful reading of the manuscript.

References

[1] Lee A E, Jost S, Wagner C N J and Tanner L E 1985 *J. Physique Coll.* **46** C8
[2] Mizoguchi T, Yoda S, Akutsu N, Yamada S, Nishioka S, Suenara T and Watanabe N 1985 *Rapid Quenched Mater.* **51** 483
[3] Fuoss P 1980 *SSRL Report No. 80/06*
[4] Fuoss P H, Eisenberger P, Warburton W and Biennenstock A 1981 *Phys. Rev. Lett.* **46** 537
[5] Shevchik N J 1977 *Phil. Mag.* **35** 805
[6] Shevchik N J 1977 *Phil. Mag.* **35** 1289
[7] de Lima J C, Raoux D, Charreire Y and Maurer M 1988 *Z. Phys. Chem. N F* BD **157** 65
[8] de Lima J C, Tonnerre J M and Raoux D 1988 *J. Non-Cryst. Solids* **106** 38
[9] Munro R 1982 *Phys. Rev.* B **25** 5037
[10] Lefebvre S, Harmelin M, Quivy A, Bigot J and Calvayrac Y 1988 *Z. Phys. Chem.* **157** 365
[11] de Lima J C 1989 *PhD Thesis* Universite de Paris-Sud, Centre d'Orsay
[12] de Lima J C, Raoux D, Tonnerre J M, Udron D, Morrison T I, Machado K D, Grandi T A and de Campos C E M 2003 *Phys. Rev.* B **67** 094210
[13] Faber T E and Ziman J M 1965 *Phil. Mag.* **11** 153

[14] Tucker M G, Dove M T and Keen D A 2002 Total scattering and reverse Monte Carlo modeling of disordered crystalline materials *From Semiconductors to Proteins: Beyond the Average Structure* (*Fundam. Mater. Res. Ser.*) ed S J L Billinge and M F Thorpe (New York: Kluwer Academic–Plenum) pp 85–103
[15] Lorch E 1969 *J. Phys. C: Solid State Phys.* **2** 229
[16] Klug H P and Alexander L E 1974 *X-ray Diffraction Procedures for Polycrystalline and Amorphous Materials* 2nd edn (New York: Wiley-Interscience) p 800
[17] Pusztai L 1995 *Models Chem.* **132** 99
[18] McGreevy R L, Howe M A and Wicks J D 1993 RMCA Version 3 downloaded from the site http://www.studsvik.uu.se
[19] Gazzillo D, Pastore G and Enzo S 1989 *J. Phys.: Condens. Matter* **1** 3469
[20] Paul F and Frahm R 1990 *Phys. Rev.* B **42** 10945
[21] Havinga E E, Damsma H and Hokkeling P 1972 *J. Less-Common Met.* **27** 169